Chain Flexibility and Bonding Kinetics of Zdol-TX Perfluoropolyether Lubricant Films Supported on Amorphous Carbon Surfaces

R. J. Waltman* and M. G. Shieh

IBM Storage and Technology Division, 5600 Cottle Road, San Jose, California 95193

Received August 14, 2000; Revised Manuscript Received May 4, 2001

ABSTRACT: The bonding kinetics of 11 Å films of the perfluoropolyether Zdol-TX, supported on amorphous hydrogenated (CHx) and nitrogenated (CNx) carbon surfaces, is investigated. The bonding rate for Zdol-TX is found to be significantly greater than for Zdol on identical carbon surfaces. The observed bonding kinetics is interpreted by a time-dependent rate coefficient, $k(t) = k_0 t^{-h}$. A crossover in the bonding time dependence from $t^{-0.50}$ to $t^{-1.00}$ is observed for Zdol-TX on CHx between 60 and 90 °C. The change in the time dependence is attributed to bonding occurring from either a solidlike ($t^{-0.50}$) or a confined liquidlike ($t^{-1.00}$) state. The crossover temperature for Zdol-TX is significantly lower than for Zdol 4000 on CHx but is similar to lower molecular weight Zdols on CHx, thereby establishing a molecular weight effect. Conversely, the bonding of the perfluoroether lubricants on CNx is limited to solidlike ($t^{-0.50}$) kinetics. The origins for the molecular weight and surface effects are discussed.

Introduction

Thin polymer films are widely used in boundary lubrication and protective overcoats at the solid interface; consequently, knowledge of their structure and physical properties is crucial in their applications. For ultrathin films, the high surface area-to-volume ratio causes a considerable departure of their behavior from bulk physical properties as the film thickness itself becomes an important parameter. By decreasing the thickness of the film to the length scale set by the polymers themselves, the conformations of the polymer chain are perturbed to the point where confinement restrictions can effect and even dominate the polymer physical properties.

Perfluoropolyethers (PFPEs) are a class of low molecular weight polymers ($M_n \leq \sim 6000$) that are widely used in the computer disk industry as topical lubricants for rigid magnetic media. Together with the amorphous carbon overcoat, they provide protection against wear and corrosion of the underlying magnetic film structure. Since the film thickness l_0 typically employed in these applications is on the order of ∼10−20 Å, their film thickness is comparable to their end-to-end distance, $R_{EE} \sim 2R_g$, where R_g is the radius of gyration.[1] When $l_0 \leq \sim R_{EE}$, large changes in the glass transition temperature (T_g) of ultrathin polymers have been observed.[2,3] Since the T_g is a parameter that is frequently related to the segmental mobility of a polymer, confinement effects are inferred. For PFPE films on carbon overcoats, recent studies have correlated the surface mobility of PFPEs on carbon surfaces to tribological reliability.[4,5] Consequently, the physisorption or "bonding" of the PFPE lubricant to the carbon overcoat surface,[6−9] and their subsequent confinement[10] has been the focus of recent investigations.

Previous work in the series has focused on the bonding kinetics of nanoscale (<20 Å) perfluoropolyether Zdol supported on amorphous hydrogenated and nitrogenated carbon surfaces, CHx and CNx.[9−11] These kinetic studies demonstrated that the bonding rate of Zdol to the carbon surface decreased with increasing time with a functional form that could be interpreted by a time-dependent rate coefficient, $k(t) = k_0 t^{-h}$. Waltman et al.[10,11] have found that the value for h is dependent upon the internal properties of the adsorbed Zdol such as chain flexibility, polymer−surface intermolecular interactions, and external factors such as temperature. These parameters determine the configurational entropy of the adsorbed PFPE film and impacts the lubricant structure and mobility.

The Zdol and Zdol-TX perfluoropolyether lubricant chemical structures are composed of a copolymer of perfluoromethylene oxide, CF_2O, and perfluoroethylene oxide, CF_2CF_2O, monomer units terminated by $-CH_2$-OH hydroxyl groups.

Zdol: $HO-CH_2CF_2O-[CF_2O]_x-[CF_2CF_2O]_y-CF_2CH_2-OH$

Zdol-TX: $HO-CH_2CH_2-O-CH_2CF_2O-[CF_2O]_x-[CF_2CF_2O]_y-CF_2CH_2-O-CH_2CH_2-OH$

The flexibility in the main chain is determined by the CF_2O/CF_2CF_2O ratio. The bonding kinetics of Zdol on amorphous carbon surfaces have been observed to be particularly sensitive to this *main chain* flexibility, exhibiting $t^{-0.5}$ and $t^{-1.0}$ dependences which were interpreted as bonding that occurred from either a solidlike ($t^{-0.5}$) or confined liquidlike ($t^{-1.0}$) state.[10] NMR studies of lubricants on surfaces as a function of lubricant film thickness also showed the effect of confinement in the monolayer thickness regime.[12] The importance of main chain flexibility in polymer chains and its effects on surface adsorption kinetics is well-established.[13]

In this report, we compare the bonding kinetics of Zdol-TX to and Zdol. The focal point of these studies is an investigation of how the bonding kinetics is influenced by the chain flexibility and end group structure of the perfluoropolyethers. The chemical structure differs primarily by the $-OCH_2CH_2-$ ethylene oxide structural moiety located close to the terminal $-CH_2$-OH hydroxyl end groups in Zdol-TX. The $-OCH_2CH_2-$ group affects the flexibility of the polymer chain near the $-CH_2OH$ hydroxyl end groups and their ability to adopt conformations on the carbon surface that are

10.1021/ma001418k CCC: $20.00
Published on Web 08/17/2001

compatible with bonding. This study will show that the bonding rate of Zdol-TX is significantly greater than that of Zdol on identical carbon surfaces. Nanoscopic interpretation is facilitated by ab initio quantum chemical calculations that compare the chain flexibility of the various structural moieties in Zdol and Zdol-TX. The results of the calculations will show that the energetic barrier to internal rotation about the near end group in Zdol, $-CF_2\cdots\cdots CH_2OH$, and equivalently the $-CF_2\cdots\cdots CH_2O-R$ in Zdol-TX, are comparatively large, $\sim$ 5 kcal/mol. However, chain flexibility is significantly enhanced by the additional $-OCH_2CH_2-$ groups in Zdol-TX which provides a relatively low energy rotational barrier, $\sim$1.5 kcal/mol, and hence enhanced segmental motion of the terminal hydroxyl end group in Zdol-TX. The computational results suggest the increased bonding rate in Zdol-TX originates from this additional chain flexibility.

In addition, the functional form of the bonding time dependence for Zdol-TX on CHx is temperature-dependent, undergoing a transition from $t^{-0.5}$ to $t^{-1.0}$ kinetics between 64 and 90 °C, much as observed previously for Zdol 4000 but at the significantly higher temperatue of $\sim$165 °C. The implications of the observed molecular weight (MW) effect and the bonding kinetics are discussed.

Experimental Section

The perfluoropolyether lubricants used in this work were obtained from Ausimont under the trade names Zdol 4000 and Zdol-TXS. From NMR analyses, Zdol 4000 (sample 1) has a $M_n = 3560$, 99.9% $-$OH functionality, and a CF_2O/CF_2CF_2O ratio of 1.08. Zdol 4000 (sample 2) has a $M_n = 4300$, 99.9% $-$OH functionality, and a CF_2O/CF_2CF_2O ratio of 0.97. Zdol-TX 2200 has a $M_n = 2380$, 99.1% $-$OH functionality, and a CF_2O/CF_2CF_2O ratio of 0.92.

The substrates used in these studies were 95 mm diameter computer rigid disks. These disks are comprised of a supersmooth Al$-$Mg substrate (rms roughness of $<\sim$20 Å) onto which are sputter-deposited an underlayer of Cr, a cobalt-based magnetic layer, and nominally $<\sim$100 Å of amorphous hydrogenated (CHx) and/or nitrogenated (CNx) carbon. The atomic composition of the carbon surfaces has previously been described.[9]

The lubricants were applied to the disks from solutions in perfluorohexane using the dip-coat method. All disks were coated with an initial lubricant film thickness of 11.0 $\pm$ 0.5 Å as measured by FTIR (Nicolet model 560), which was calibrated to film thickness determined by ellipsometry and/or XPS.[14] Throughout the following, we refer to the Zdol lubricant on the disk surface as either being "bonded" or "mobile". To clarify our definition of these terms, we briefly describe the methodology by which these quantities are determined. Following lubricant application, the initial Zdol thickness is measured via specular reflectance FT-IR. The lubricated disks are then annealed for a specified period of time, and the remaining Zdol film thickness is remeasured. The decrease in the lubricant thickness following annealing yields the evaporated amount. In the following, we report the evaporated fraction, which is defined as the amount evaporated normalized to the initial thickness. After annealing, the disks are washed sequentially in perfluorohexane (FC-72, 3M) and 2,3-dihydroperfluoropentane (Vertrel-XF, DuPont) or hydrofluoroether (HFE$-$7100, 3M) to remove any soluble lubricant, and the lubricant thickness is remeasured. The lubricant retained by the disk is defined to be the amount "bonded", while the portion removed by the solvent wash process is defined as the "mobile" lubricant. For bonded lubricant, our experiments do not distinguish between physi- and/or chemisorption.[9] Again, the fraction bonded and the mobile fraction are obtained by normalizing to the initial lubricant thickness.

Computational Methodology

Ab initio calculations were performed using the Gaussian 98W version 5.2 computer code.[15] The energetics associated with the rotation about the C$-$C and C$-$O bonds in Zdol and Zdol-TX were determined from Hartree$-$Fock SCF (self-consistent field) and MP2 (perturbation theory) calculations performed with the 6-31G[d] basis set.[16] For these purposes, the following model structures were employed:

ZD (Zdol model): $CF_3OCF_2CH_2-OH$

ZTX (Zdol-TX model):

$$CF_3OCF_2CH_2-OCH_2CH_2-OH$$

The torsional potential was computed for every 10° of C$-$C or C$-$O rotation where the structures were fully optimized at each torsion angle. Figures reproducing the optimized geometries were made using the CambridgeSoft Chem3D molecular modeling program.[17]

Results

Bonding Kinetics. The bonding kinetics for Zdol 4000 and Zdol-TX 2200 on CNx, at 20 and 64 °C, are presented in Figures 1 and 2. The theoretical fits accompanying the kinetic data, shown as the solid lines in the figures, are developed assuming a rate coefficient that is time-dependent, i.e., $k(t) \propto k_0 t^{-h}$. Thus, the differential rate equations for the depletion of mobile Zdol, A, the formation of bonded Zdol, B, and the evaporation of mobile Zdol, C, for any value of the time dependence h may be written as

$$\frac{dB}{dt} = k(t)A = k_B t^{-h} A \tag{1}$$

$$\frac{dC}{dt} = k(t)A = k_C t^{-h} A \tag{2}$$

$$-\frac{dA}{dt} = \frac{dB}{dt} + \frac{dC}{dt} \tag{3}$$

where k_B and k_C are the initial rate coefficients for the bonding and evaporation reactions, respectively. For the bonding studies conducted here, $h = 0.50-1.00$ for Zdol (Zdol-TX) on CHx and $h = 0.50$ for Zdol (Zdol-TX) on CNx in eq 1. For evaporation of Zdol (Zdol-TX) on CHx and CNx, $h = 1.00$ in eq 2. The significance of the functional form of the time dependence and the magnitude for h have been discussed previously[10] and are not the focal point of this paper. Briefly, the bonding kinetics described by $h = 0.50$ is interpreted to arise from a solidlike Zdol film limited by a random walk confined to one dimension as described by Kopelman et al.[18] When $h = 1.00$, the bonding kinetics occurs from a liquidlike Zdol film indicative of segmental mobility governed by barriers to internal rotation about specific bonds. Similar bonding time dependences have been observed previously[19] for both polydispersed and narrowly dispersed perfluoropolyethers, exhibiting great sensitivity to both surface composition[9] and chain flexibility.[10]

Bonding Data. In Figure 1, the changes in the mobile, bonded, and evaporated fractions for Zdol 4000 and Zdol-TX 2200 as a function time at ambient conditions, i.e., 20 °C and 50 $\pm$ 10% relative humidity, are compared. Referring to the bonding of the Zdols on CNx,

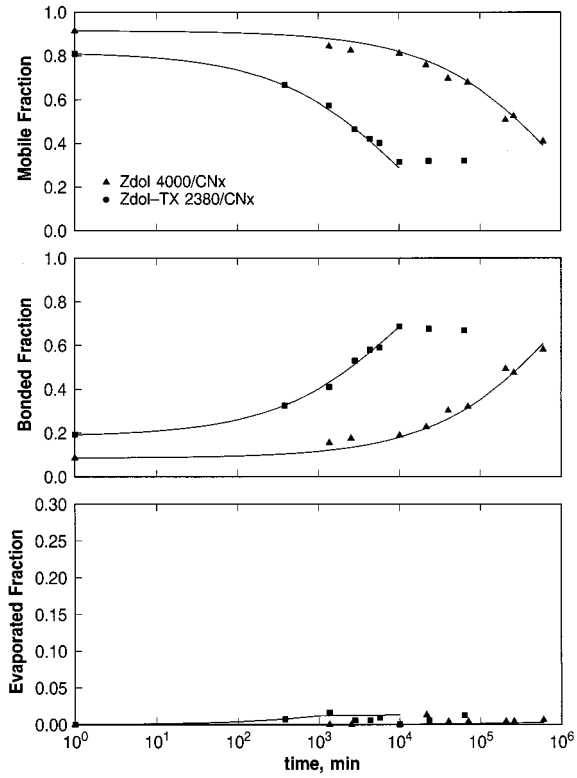

Figure 1. Changes in the (top) mobile, (middle) bonded, and (bottom) evaporated fractions of Zdol 4000 and Zdol-TX 2200 on CNx as a function of time at 20 °C and 50 ± 10% relative humidity. All initial film thicknesses were 11.0 ± 0.5 Å. The solid lines accompanying the data points are obtained from the theoretical fits of eqs 1−3 using $h = 0.50$ and 1.00 for bonding and evaporation, respectively. For Zdol 4000, $k_B = 5.5 \times 10^{-4}$ and $k_C = 3.0 \times 10^{-6}$; for Zdol-TX 2200, $k_B = 5.2 \times 10^{-3}$ and $k_C = 3.0 \times 10^{-4}$.

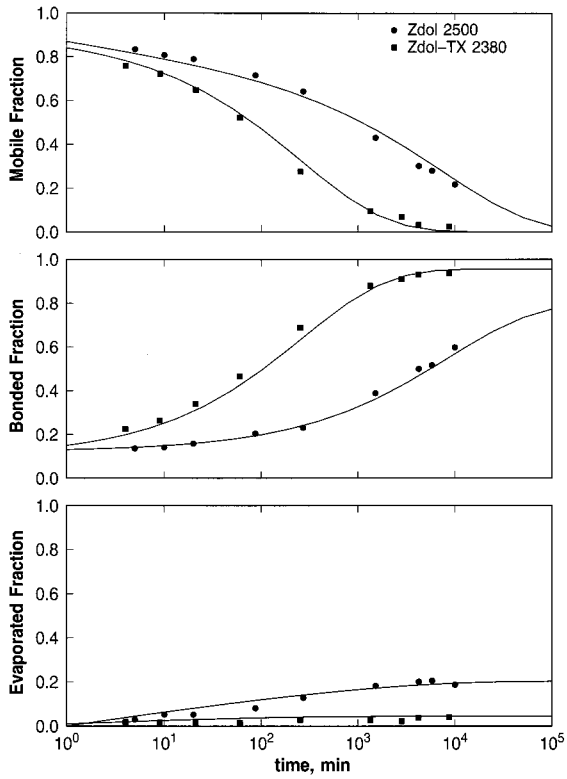

Figure 2. Changes in the (top) mobile, (middle) bonded, and (bottom) evaporated fractions of Zdol 2500 and Zdol-TX 2200 on CNx as a function of time at 64 °C and 4% relative humidity. All initial film thicknesses were 11.0 ± 0.5 Å. The solid lines accompanying the data points are obtained from the theoretical fits of eqs 1−3 using $h = 0.50$ and 1.00 for bonding and evaporation, respectively. For Zdol 2500, $k_B = 5.0 \times 10^{-3}$ and $k_C = 3.3 \times 10^{-2}$; for Zdol-TX 2200, $k_B = 3.0 \times 10^{-2}$ and $k_C = 8.5 \times 10^{-3}$.

Figure 1 (middle), the bonding rate for Zdol-TX is observed to be significantly greater than for Zdol. Under ambient conditions, both Zdols attain a maximum bonded level of approximately 60−70%. However, the time required to reach this bonded level is only 10^4 min (∼7 days) for Zdol-TX compared to 10^5−10^6 min (>∼100 days) for Zdol. The theoretical treatment, eqs 1−3, provides an excellent fit of the experimental data points up to the maximum bonded level. This is to be contrasted in Figure 2 where, at the higher temperature of 64 °C and a lower relative humidity of 4%, all of the mobile lubricant remaining on the disk eventually becomes bonded. In Figure 2, we compare Zdol 2500 (CF_2O/CF_2CF_2O, or "C1/C2" ratio of 0.87) and Zdol-TX (C1/C2 = 0.92) because of their similar MW and structural composition of the main chain, thereby isolating structural effects due to the $-CF_2CH_2-OH$ and the $-CF_2CH_2-O-CH_2CH_2-OH$ end groups. Under these conditions, both bonding data are completely fit using $h = 0.50$ in eq 1. Thus, as evidenced in Figure 2 (middle), the characteristic feature of the $k(t) \propto k_0 t^{-0.5}$ bonding kinetics is an asymptotic limit of 100% bonded lubricant on the disk and complete depletion of mobile lubricant (Figure 2, top). Again, Zdol-TX attains a completely bonded state after a significantly shorter time, $\sim 10^3$ min compared to $\sim 10^5$ min for Zdol.

In Figure 3, the changes in the mobile, bonded, and evaporated fractions for 11 Å of Zdol-TX on CHx, as a function time, between 64 and 150 °C are presented. Referring to the bonding kinetics, Figure 3 (middle), the bonding rate coefficients are observed to increase with

Table 1. Rate Coefficients for the Bonding and Evaporation of Zdol-TX 2200 on CHx and CNx as a Function of Temperature[a]

temp, °C	CHx			CNx		
	k_B	k_C	h (bonding)	k_B	k_C	h (bonding)
64	0.020	0.0153	0.50	0.0300	0.0085	0.50
90	0.094	0.049	0.79	0.101	0.029	0.50
120	0.303	0.108	1.00	0.225	0.072	0.50
150	0.480	0.190	1.00	0.307	0.160	0.50

[a] h is the heterogeneity index that determines the time dependence of the bonding reaction, t^{-h}.

temperature (Table 1). With increasing temperature, the functional form of the time dependence is also observed to change. At 64 °C, the theoretical fit using $k(t) \propto k_0 t^{-0.5}$ provides an excellent fit of the experimental data points. At 120 and 150 °C, the kinetic data are observed to fit the $k(t) \propto k_0 t^{-1.0}$ theoretical dependence, and the shapes of the bonding profiles are observed to change significantly from the $k(t) \propto k_0 t^{-0.5}$ fit. For $k(t) \propto k_0 t^{-1.0}$ bonding, there is a rapid initial rise in the bonded fraction and a gradual decrease in the rate coefficient charaterized by the inverse time dependence. The initial portion of the bonding profile is concave to the time axis. For $k(t) \propto k_0 t^{-0.5}$ bonding, there is a comparatively slower rise in the initial bonded fraction and the initial bonding curve is convex to the time axis. Between the two extremes of $h = 0.5$ at 64 °C and $h = 1.0$ at 120 °C, a "crossover" in the time dependence of the bonding kinetics is observed. The best theoretical fit is obtained using $k(t) \propto k_0 t^{-0.79}$, where the theoretical rate curve

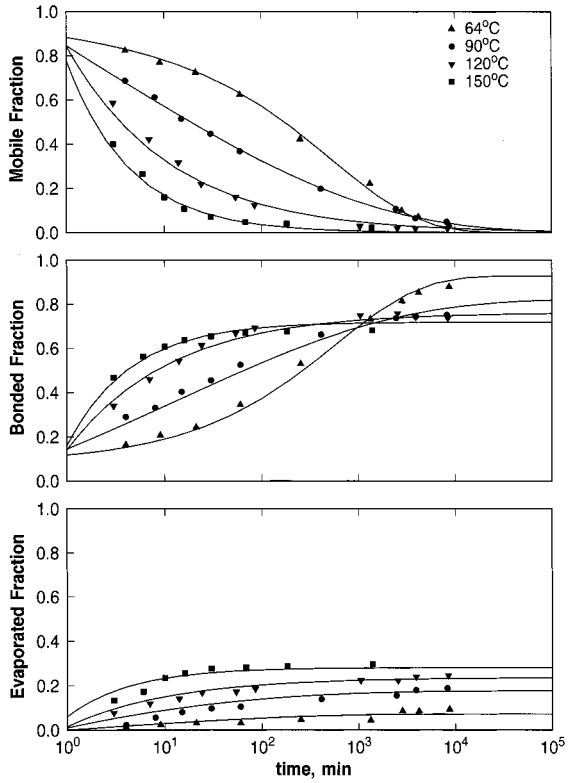

Figure 3. Changes in the (top) mobile, (middle) bonded, and (bottom) evaporated fractions of Zdol-TX 2200 on CHx as a function of time and temperature and ≤4% relative humidity. All initial film thicknesses were 11.0 ± 0.5 Å. The solid lines accompanying the data points are obtained from the theoretical fits of eqs 1−3 using the *h* values indicated in Table 1.

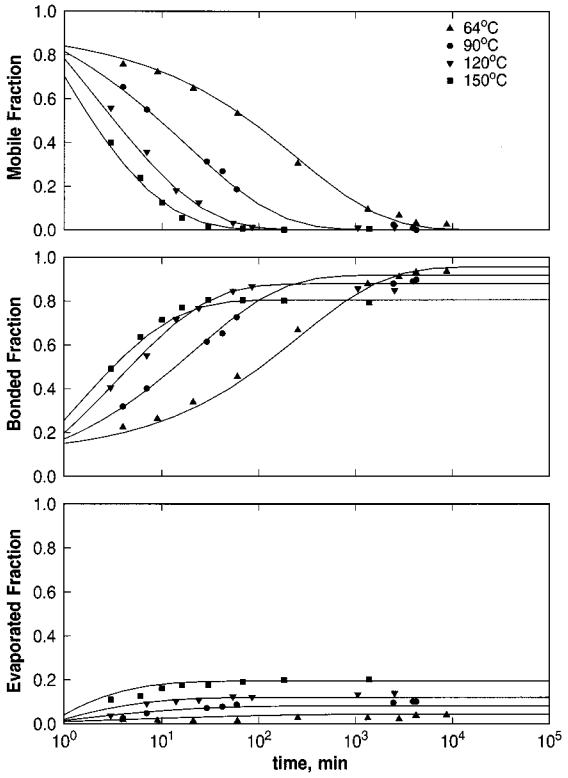

Figure 4. Changes in the (top) mobile, (middle) bonded, and (bottom) evaporated fractions of Zdol-TX 2200 on CNx as a function of time and temperature and ≤4% relative humidity. All initial film thicknesses were 11.0 ± 0.5 Å. The solid lines accompanying the data points are obtained from the theoretical fits of eqs 1−3 using the *h* values indicated in Table 1.

now coincides with the experimental data points. Since the bonding reaction occurs in parallel to evaporation, $h = 0.79$ for bonding and $h = 1.00$ for evaporation reproduces the overall loss of mobile lubricant, Figure 3 (top).

The evaporation and bonding kinetics for Zdol-TX on CNx, between 64 and 150 °C, are presented in Figure 4. In contrast to the bonding on CHx, the bonding on CNx are all readily fit by the $k(t) \propto k_0 t^{-0.5}$ time dependence in the bonding channel. Thus, unlike Zdol-TX on CHx, a transition in the functional form of the bonding time dependence is not observed in the temperature range investigated. The rate coefficients and time dependences for the bonding and evaporation of Zdol-TX on both CHx and CNx are summarized in Table 1.

Ab Initio Calculations. The optimized geometries for our Zdol models, ZD and ZTX, are presented in Figure 5. While not the focal point of this investigation, the results demonstrate that, in the perfluoromethyl group centered at C1, the C−F bond closest to the C−O−C plane is rotated out of the plane by 17.4°. This is characteristic of polyperfluorinated ether structures containing the C−O−C backbone and is a result of the interaction between the lone pairs of electrons on the fluorine and oxygen atoms. The structural details for the optimized geometry for ZD are consistent with previous experimental and theoretical studies of structurally similar perfluorinated ether models.[20]

The calculated energy map for rotation about the C6−C7 bond in ZD, presented in Figure 6 (top), demonstrates that when the C−H and C−F bonds are staggered at −180° and ±60°, local energy minima exist.

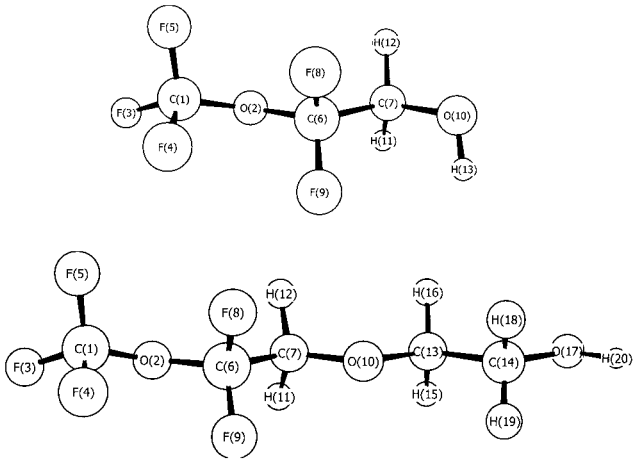

Figure 5. SCF/6-31G[d] optimized geometries for ZD and ZTX.

Because all geometric parameters are optimized, these minima represent the stable conformers of ZD. Energy maxima in ZD occur when the C−F and C−O bonds are eclipsed at ±120° and when the C−O bonds (C7−O10, C6−O2 in Figure 5) are eclipsed at ∼0°. From the data presented in Figure 6 (top), rotation about the C6−C7 bond is estimated to be ∼5.5 kcal/mol, at both SCF and MP2 levels of theory. Thus, rotation of the C−C bond adjacent to the $-CH_2OH$ end group is relatively confined.

The calculated energy map for rotation about the C6−C7 bond in ZTX, presented in Figure 6 (bottom), is both qualitatively and quantitatively very similar to the torsional potential for ZD for the same bond rotation.

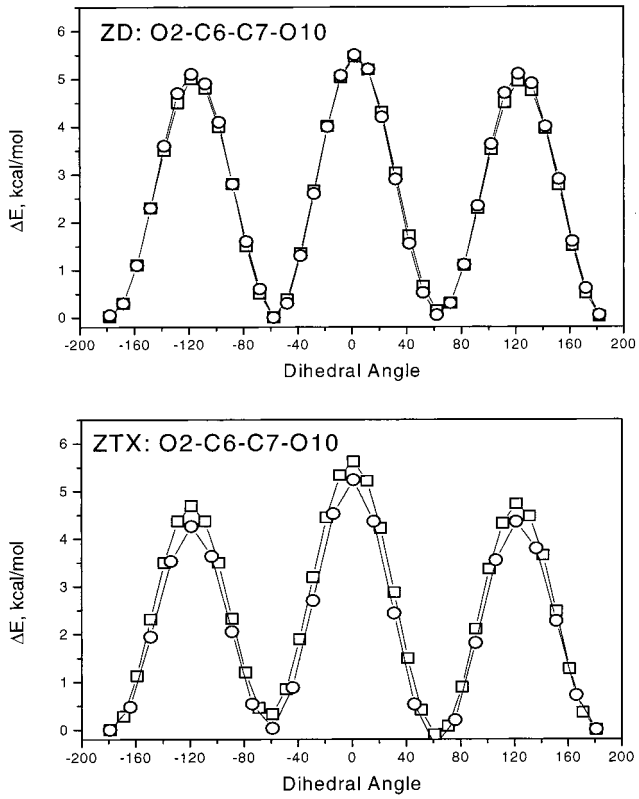

Figure 6. Torsional potentials and optimized geometries for the C−C rotation in ZD (top) and ZTX (bottom) as a function of the O10−C7−C6−O2 dihedral angle: (□) SCF/6-31G[d] and (○) MP2/6-31G[d].

Energy minima occur when the C7−O bond is staggered to the C6−O and C6−F bonds at −180° and ±60°. Referring to the optimized geometry presented in Figure 5, energy maxima occur when the C6−F and C7−O bonds are eclipsed at ±120° and when the C−O bonds (C7−O10, C6−O2 in Figure 5) are eclipsed at ∼0°. At the ±120° maxima, the F−C6−C7−O10 dihedral angle is ∼0°, with a F−O10 nonbonding close contact of 2.5 Å. At the 0° maximum, the O2−C6−C7−O10 dihedral angle is ∼0°, with a nonbonding close contact of 2.5 Å. The rotation about the C6−C7 bond is computed to be ∼5 kcal/mol and may be considered to be relatively stiff, virtually identical to the corresponding ZD structural moiety. Interestingly, the optimized geometry presented for the C6−C7 rotation at 61° is the global minimum on the potential energy surface. This is attributed to an "oxygen gauche effect"[17] in perfluorinated RO−C−C−OR structures that can introduce a "kink" in the main chain. Implications to the adsorbed film structure have been discussed previously.[11]

The calculated energy map for rotation about the C7−O10 bond in ZTX is presented in Figure 7 (top). The 3-fold potential barrier is characterized by two relatively small maxima at 130° and 220° of ∼1−1.5 kcal/mol and a significantly larger ∼7 kcal/mol barrier at 0°. There is considerable chain flexibility in this bond rotation from approximately 60° to 300° in the C6−C7−O10−C13 dihedral angle. The small barrier at 130° (220°) does not have a large steric contribution. The nonbonding interatomic distances are comparable to the optimized ZTX geometry (Figure 5) with the exception of closer contacts between H15 and F9 of 3.3 Å instead of 4.3 Å at 130° and 3.3 Å instead of 4.3 Å between H16 and F8 at 220°. However, at the 7 kcal/mol barrier

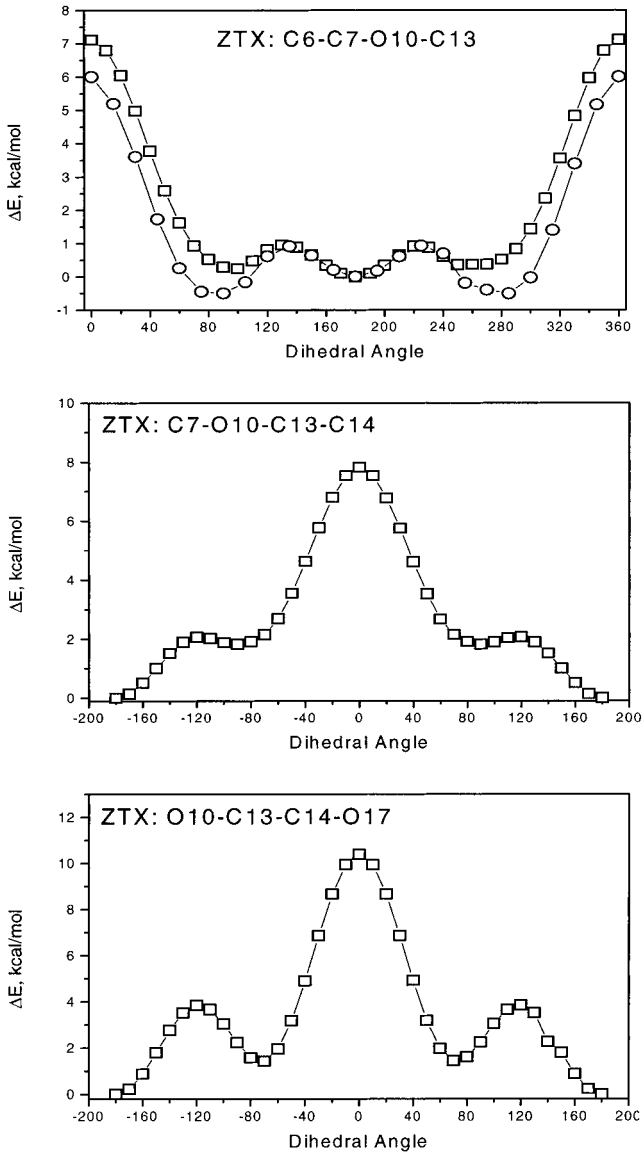

Figure 7. Torsional potentials and optimized geometries for the bond rotations in ZTX as a function of (top) the C13−O10−C7−C6 dihedral angle, (□) SCF/6-31G[d], (○) MP2/6-31G[d]; (middle) the C14−C13−O10−C7 dihedral angle, (□) SCF/6-31G[d]; and (bottom) the O1−C14−C13−O10 dihedral angle, (□) SCF/6-31G[d].

maximum, the local C6−C7−O10−C13 geometry is planar, with steric energy arising from the nonbonding close contacts between the eclipsed C6−F and C13−H bonds of 2.45 Å. Thus, rotation of the $-CH_2OH$ end group via the C7−O10 bond is relatively unconfined between 60° and 300° and imparts a large degree of configurational freedom in the $-CH_2OH$ end group, in contrast to the near end group C6−C7 rotations discussed previously.

The calculated energy map for rotation about the O10−C13 bond in ZTX is presented in Figure 7 (middle). The 3-fold potential barrier is characterized by a relatively large 8 kcal/mol energy barrier at 0°, surrounded by two relatively shallow minima of ∼1.8 kcal/mol at ±90° and two maxima of ∼2 kcal/mol at ±120°. In comparison to the stiff C6−C7 and the more flexible C7−O10 bond rotations considered peviously, the O10−C13 bond provides a relatively stiff barrier to internal rotation. The lower energy maxima at ±90° is characterized by nonbonding close contacts between C14−H

and O10 of 2.6 Å. At the 8 kcal/mol barrier maximum, the local C7−O10−C13−C14 geometry is planar, with steric energy arising from the nonbonding close contacts of the eclipsed C7−H and C14−H bonds at 2.38 Å.

The calculated energy map for rotation about the C13−C14 bond in ZTX is presented in Figure 7 (bottom). The 3-fold potential barrier is characterized by a relatively large 10 kcal/mol energy barrier at 0°, surrounded by two minima of ∼1.5 kcal/mol at ±90° and two maxima of ∼4 kcal/mol at ±120°. The lower energy maxima at ±120° is characterized by nonbonding close contacts between the eclipsed C13−H and C14−O of 2.3 Å. At the 10 kcal/mol barrier maximum, the local O10−C13−C14−O17 geometry is planar, with steric energy arising from the nonbonding close contacts of the eclipsed C−O bonds at 2.5 Å. Thus, rotation of the $-CH_2OH$ end group via the C13−C14 bond is considered to be sterically hindered.

Discussion

The data presented in Figures 1 and 2 establish the significantly higher bonding rate for Zdol-TX compared to Zdol on identical carbon surfaces. Previous studies by contact angle goniometry[21] have shown that the bonding reaction requires the spatial delivery of the −OH hydroxyl end groups in Zdol to the suitable active sites on the carbon surface. For the bonding reaction to occur, the Zdol −OH end groups must be within the capture radius of the surface active site, and this may be achieved by internal rotations about C−C and C−O bonds. Since the carbon surfaces used in the comparative bonding studies are identical, we expect the higher bonding rate in Zdol-TX to be associated with the more flexible $-O-CH_2-CH_2-$ structural moiety even at the lower temperature where the bonding occurs from a more solidlike Zdol state (Figure 1).

The data presented in Figure 3 on the bonding of Zdol-TX (CF_2O/CF_2CF_2O, or "C1/C2" ratio of 0.92) on CHx indicate a change in the functional form of the time dependence from $t^{-0.50}$ to $t^{-1.00}$ nominally near 90 °C. A similar transition has already been effected for Zdol 4000 (C1/C2 ratio of 0.97) on CHx at nominally ∼165 °C as a function of the main chain flexibility and temperature.[10] This change in the bonding time dependence has been interpreted previously as bonding arising from a solidlike ($t^{-0.50}$) and a confined liquidlike ($t^{-1.00}$) adsorbed Zdol. While beyond the scope of this paper, both Zdol 2500 and 1350 MW, with CF_2O/CF_2CF_2O ratios < 1, also exhibit a change in the bonding time dependence from $t^{-0.50}$ to $t^{-1.00}$ kinetics. (Zdol 2500 and 1350 are structurally analogous to Zdol 4000 and mainly differs in molecular weight.) In both cases, the temperature at which the bonding time dependence crosses over from $t^{-0.50}$ to $t^{-1.00}$ occurs in the significantly lower 60−90 °C range. This indicates that, in addition to main chain flexibility and temperature, MW can also be a strong determinant of the functional form of the bonding time dependence, i.e., t^{-h}, as summarized in Figure 8. In Figure 8 (top), the dependence of h in t^{-h} for the bonding kinetics (eq 1) on the main chain flexibility of Zdol 4000 (C1/C2 ratio) is indicated. As the C1/C2 ratio is increased, bonding is more likely to occur via the $t^{-1.00}$ kinetics. Chain flexibility is apparently an important parameter even in confined films as measured by the bonding kinetics. In Figure 8 (middle), the dependence of h in t^{-h} for the bonding kinetics (eq 1) as a function of temperature is

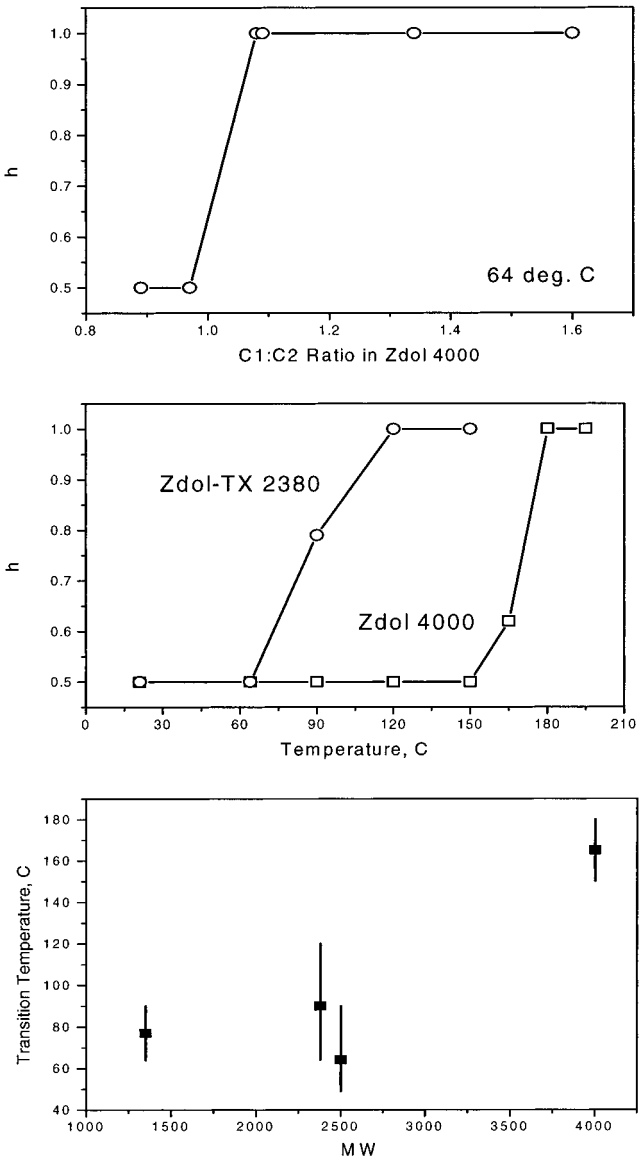

Figure 8. (top) Dependence of h in t^{-h} for the bonding kinetics, eq 1, for Zdol 4000 as a function of the CF_2O/CF_2CF_2O ratio. (middle) The dependence of h in t^{-h} for the bonding kinetics, eq 1, for Zdol 4000 (C1/C2 = 0.97) and Zdol-TX 2200 (C1/C2 = 0.92) as a function of temperature. (bottom) The dependence of the temperature at which the bonding time dependence changes from $t^{-0.50}$ to $t^{-1.00}$ for Zdols as a function of M_n. Zdol 1350 with C1/C2 = 0.93; Zdol-TX 2200 with C1/C2 = 0.92; Zdol 2500 with C1/C2 = 0.87; Zdol 4000 with C1/C2 = 0.97.

compared for Zdol 4000 and Zdol-TX with C1/C2 ratios of 0.97 and 0.92, respectively. At the same film thickness, a decrease in MW causes a significant decrease in the temperature range at which the $t^{-0.50}$ kinetics crosses over to the $t^{-1.00}$ kinetics. This aspect is summarized in Figure 8 (bottom), where the MW dependence of the $t^{-0.50}$ to $t^{-1.00}$ transition temperature is presented for various Zdols with M_n of 1350 (C1/C2 = 0.93), 2500 (C1/C2 = 0.87), and 4000 (C1/C2 = 0.97), in addition to the Zdol-TX (C1/C2 = 0.92). The bottom and top of the vertical bars in the figure are indicative of the onset and completion of the $t^{-0.50}$ to $t^{-1.00}$ temperature transition, respectively. On the basis of these data, we might expect the decrease in the temperature of the $t^{-0.50}$ to $t^{-1.00}$ bonding kinetics transition from ∼165 °C in Zdol 4000 to ∼90 °C in Zdol-TX 2200 (and between ∼60 and 90 °C for Zdol 2500, 1350 MW; Figure 8) as

arising from an interplay between confinement effects and increased mobility via the increasing number density of end groups with decreasing MW. These data are consistent with previously measured Zdol film disjoining pressures which were observed to increase with increasing MW in the ~11 Å regime.[22] It is expected that the entropy decrease as a result of the film confinement (increasing disjoining pressure) shifts the temperature of transition to higher values.

Interestingly, a change in the functional form of the time dependence is not observed for Zdol-TX on CNx (Figure 4), at least in the same temperature range investigated for CHx. Thus, for all temperatures between 20 and 150 °C, the bonding rate coefficient is described by $k(t) \propto k_0 t^{-0.5}$. We have previously shown that the intermolecular interactions between Zdol and CNx are more repulsive than Zdol on CHx.[9] The Zdol−CNx interaction is characterized by a negative Hamaker constant.[9] Furthermore, surface titration studies indicated more Zdol could access the CNx surface compared to CHx, thereby increasing the Zdol packing in the adsorbed monolayer on CNx.[9,11] The increased packing could result in the loss of configurational entropy causing confinement restriction and hence may account for the observed $t^{-0.5}$ bonding kinetics on CNx.

Concluding Remarks

The bonding kinetics of Zdol-TX on amorphous carbon surfaces were investigated. The bonding rate coefficient for Zdol-TX was found to be significantly greater than Zdol on identical carbon surfaces. These data were interpreted on the basis of the relative chain flexibility of Zdol and Zdol-TX. It was found that the additional $-OCH_2CH_2-$ groups in Zdol-TX provided a relatively low energy rotational barrier near the terminal hydroxyl end group, ~1.5 kcal/mol compared to ~5 kcal/mol for Zdol, whereupon it was concluded that Zdol-TX conformations that were more compatible to bonding could be more easily accessed. However, the time dependence in the observed kinetics, $k(t) = k_0 t^{-h}$, was dominated by main chain flexibility.

A significant reduction in the temperature required to effect a transition from $t^{-0.50}$ to $t^{-1.00}$ bonding kinetics was found for Zdol-TX on CHx compared to Zdol 4000 on CHx. Since the CF_2O/CF_2CF_2O ratio for Zdol 4000 and Zdol-TX was $<\sim 1$, indicative of relatively stiff chains, and a similar temperature reduction has been recently observed in both Zdol 2500 and 1350 MWs, the reduction in the transition temperature was attributed primarily to a molecular weight effect. On CNx, a similar transition in the time dependence of the bonding kinetics could not be induced between 20 and 150 °C, due to differences in the polymer−surface intermolecular interactions and the adsorbed film structure.

This work vividly illustrates the complicated nature of nanoscopic films supported on surfaces. While these types of systems are technologically important, molecular level details that can affect functional performance are often not necessarily well-understood. An interplay of the internal parameters of polymers such as chain flexibility and configurational entropy, polymer−surface interactions, surface-to-volume ratios, and external control parameters such as temperature are all significant determinants in nanoscale films. The resultant properties of the adsorbed film depend on which of these parameters is dominant.

References and Notes

(1) Cotts, P. M. *Macromolecules* **1994**, *27*, 6487.

(2) (a) Forrest, J. A.; Dalnoki-Veress, K.; Dutcher, J. R. *Phys. Rev. E* **1997**, *56*, 5705. (b) Wallace, W. E.; van Zanten, J. H.; Wu, W.-L. *Phys. Rev. E* **1995**, *52*, 3329. (c) van Zanten, J. H.; Wallace, W. E.; Wu, W.-L. *Phys. Rev. E* **1996**, *53*, 2053. (d) Forrest, J. A.; Svanberg, C.; Révész, K.; Rdahl, M.; Torell, L. M.; Kasemo, B. *Phys. Rev. E* **1998**, *58*, 1226. (e) Forrest, J. A.; Dalnoki-Veress, K.; Stevens, J. R.; Dutcher, J. R. *Phys. Rev. Lett.* **1996**, *77*, 2002. (f) Keddie, J. L.; Jones, R. A. L.; Cory, R. A. *Faraday Discuss.* **1994**, *98*, 219. (g) Liu, Y.; Russell, T. P.; Samant, M. G.; Stöhr, J.; Brown, H. R.; Cossy-Favre, A.; Diaz, J. *Macromolecules* **1995**, *28*, 6808. (h) Satomi, N.; Takahara, A.; Kajiyama, T. *Macromolecules* **1999**, *32*, 4474.

(3) (a) Mansfield, K. F.; Theodorou, D. N. *Macromolecules* **1991**, *24*, 6283. (b) Baschnagel, J.; Binder, K. *Macromolecules* **1991**, *24*, 6283. (c) Thompson, P. A.; Grest, G. S.; Robbins, M. O. *Phys. Rev. Lett.* **1992**, *68*, 3448.

(4) Wang, R.-H.; White, R. L.; Meeks, S. W.; Min, B. G.; Kellock, A.; Homola, A.; Yoon, D. *IEEE Trans. Magn.* **1996**, *32*, 3777.

(5) Khurshudov, A.; Baumgart, P.; Waltman, R. J. *Wear* **1999**, *225−229*, 690.

(6) (a) Perry, S. S.; Somorjai, G. A.; Mate, C. M.; White, R. *Tribol. Lett.* **1995**, *1*, 47. (b) Perry, S. S.; Merrill, P. B.; Kim, H. I. *Tribol. Lett.* **1996**, *2*, 393.

(7) Cornaglia, L. M.; Gellman, A. J. *J. Vac. Sci. Technol. A* **1997**, *15*, 2755.

(8) Mate, C. M. *Tribol. Lett.* **1998**, *4*, 119.

(9) (a) Waltman, R. J.; Pocker, D.; Tyndall, G. W. *Tribol. Lett.* **1998**, *4*, 267. (b) Tyndall, G. W.; Waltman, R. J.; Pocker, D. *Langmuir* **1998**, *14*, 7527. (c) Waltman, R. J.; Tyndall, G. W.; Pacansky, J. *Langmuir* **1999**, *15*, 6470.

(10) Waltman, R. J.; Tyndall, G. W.; Pacansky, J.; Berry, R. J. *Tribol. Lett.* **1999**, *7*, 91.

(11) Waltman, R. J.; Zhang, H.; Khurshudoz, A.; Pocker, D.; Karplus, M.; York, B.; Xiao, Q.-F.; Zadoori, H.; Thiele, J.-U.; Tyndall, G. W. *Tribol. Trans.*, submitted for publication.

(12) Yanagisawa, M. *Tribol. Trans.* **1994**, *37*, 629.

(13) (a) Silberberg, A. *J. Chem. Phys.* **1967**, *46*, 1105. (b) Silberberg, A. *J. Phys. Chem.* **1962**, *66*, 1872. (c) Silberberg, A. *J. Phys. Chem.* **1962**, *66*, 1884. (d) Hoeve, C. A.; DiMarzio, E. A.; Peyser, P. *J. Chem. Phys.* **1965**, *42*, 2558.

(14) Toney, M. F.; Mate, C. M.; Pocker, D. J. *IEEE Trans. Magn.* **1998**, *34*, 1774.

(15) Frisch, M. J.; Trucks, G. W.; Schlegel, H. B.; Scuseria, G. E.; Robb, M. A.; Cheeseman, J. R.; Zakrzewski, V. G.; Montgomery, J. A., Jr.; Stratmann, R. E.; Burant, J. C.; Dapprich, S.; Millam, J. M.; Daniels, A. D.; Kudin, K. N.; Strain, M. C.; Farkas, O.; Tomasi, J.; Barone, V.; Cossi, M.; Cammi, R.; Mennucci, B.; Pomelli, C.; Adamo, C.; Clifford, S.; Ochterski, J.; Petersson, G. A.; Ayala, P. Y.; Cui, Q.; Morokuma, K.; Malick, D. K.; Rabuck, A. D.; Raghavachari, K.; Foresman, J. B.; Cioslowski, J.; Ortiz, J. V.; Stefanov, B. B.; Liu, G.; Liashenko, A.; Piskorz, P.; Komaromi, I.; Gomperts, R.; Martin, R. L.; Fox, D. J.; Keith, T.; Al-Laham, M. A.; Peng, C. Y.; Nanayakkara, A.; Gonzalez, C.; Challacombe, M.; Gill, P. M. W.; Johnson, B. G.; Chen, W.; Wong, M. W.; Andres, J. L.; Head-Gordon, M.; Replogle, E. S.; Pople, J. A. *Gaussian 98*, revision x.x; Gaussian, Inc.: Pittsburgh, PA, 1998.

(16) Raghavachari, K.; Pople, J. A. *Int. J. Quantum Chem.* **1981**, *20*, 1067.

(17) CS ChemOffice, Cambridge Soft Corporation 1997, Cambridge, MA 02139.

(18) (a) Argyrakis, P.; Kopelman, R.; Lindenberg, K. *Chem. Phys.* **1993**, *177*, 693. (b) Kopelman, R. *Science* **1988**, *241*, 1620.

(19) Tyndall, G. W.; Waltman, R. J. *J. Phys. Chem.* **2000**, *104*, 7085.

(20) (a) Stanton, C. L.; Schwartz, M. *J. Phys. Chem.* **1993**, *97*, 11221. (b) Stanton, C. L.; Paige, H. L.; Schwartz, M. *J. Phys. Chem.* **1993**, *97*, 5901. (c) Stanton, C. L.; Berry, R. J.; Schwartz, M. *J. Phys. Chem.* **1995**, *99*, 3473. (d) Smith, G. D.; Jaffe, R. L.; Yoon, D. Y. *Macromolecules* **1995**, *28*, 5804.

(21) Tyndall, G. W.; Leezenberg, P. B.; Waltman, R. J.; Castenada, J. *Tribol. Lett.* **1998**, *4*, 103.

(22) Tyndall, G. W.; Karis, T. E.; Jhon, M. S. *Tribol. Trans.* **1999**, *3*, 463.

MA001418K